Construction and Building Materials 411 (2024) 134243

Contents lists available at ScienceDirect

Construction and Building Materials

journal homepage: www.elsevier.com/locate/conbuildmat

Effect of hydrogel on mitigating drying shrinkage induced cracking in carbonation cured calcium silicate binders

Elvis Baffoe, Ali Ghahremaninezhad *

Department of Civil and Architectural Engineering, University of Miami, Coral Gables, FL 33146, United States

ARTICLE INFO

Keywords:
Hydrogel
Wollastonite
Carbonation
Drying shrinkage

ABSTRACT

Carbonation cured calcium silicate binders can be considered an alternative material to reduce the carbon footprint of the construction industry. Carbonation at elevated temperatures is used to enhance carbonation reaction; however, it accelerates drying, which could result in drying shrinkage induced cracking. The effect of hydrogel on the microstructure and properties of carbonated wollastonite pastes was discussed in this paper. The teabag test and flow test showed that hydrogel absorption was notably higher in wollastonite paste than in OPC paste. The phase analysis based on Fourier transform infrared spectroscopy (FTIR), X-ray diffraction (XRD), and thermogravimetric analysis (TGA), revealed calcite as the primary polymorph of calcium carbonate in the carbonated product. The micro-CT analysis showed crack formation in the control pastes while no or significantly fewer cracks were observed in the hydrogel modified pastes. The hydrogel modified pastes exhibited lower water loss and drying shrinkage compared to the control paste at early carbonation stage. The above results provided evidence that cracking was caused by drying shrinkage in the control carbonated pastes and hydrogel was effective in mitigating such cracking by lowering water loss at early stage of carbonation. The results of the nitrogen adsorption test indicated a higher specific surface area and pore volume in the hydrogel modified pastes. The hydrogel modified pastes exhibited a slightly reduced compressive strength due to the presence of hydrogel macrovoids in these pastes.

1. Introduction

Cement-based materials account for about 9% of the global greenhouse gas emissions. In addition, the industrial production of 1 ton of ordinary Portland cement (OPC) requires 4–5 GJ of energy, which approximates to about 5% of the industrial energy consumption globally [1]. The carbon dioxide emanates from the decomposition of limestone and firing of the clinker phases at the high temperature of about 1450 °C to produce Portland cement [2]. Due to these environmental effects, other alternative binder materials with low carbon footprints and smaller embodied energy have been at the center of investigations for years. One of such alternative binders is the carbon-dioxide activated calcium silicates such as wollastonite.

Wollastonite is a non-hydraulic, low-lime calcium silicate binder which is hardened when calcium silicates ($CaO.SiO_2$, [CS]) react with carbon dioxide in the presence of moisture. The reaction leads to the formation of calcium carbonate and calcium-modified silica gel [2,3] following the two steps shown below:

$$CO_2 + H_2O \leftrightarrow H^+ + HCO_3^- \quad (1)$$

$$mCaO.nSiO_2 + xH^+ + xHCO_3^- \leftrightarrow yCaO.nSiO_2 + (m-y)CaCO_3 + xH_2O \quad (2)$$

These reaction products act as the binding phases to provide the strength of the hardened mixture. The production temperature of the calcium silicates is about 250 °C lower than that of OPC [4]. The amount of limestone needed for producing wollastonite is less than that required for producing OPC. Thus, the production of wollastonite-based binders involves less carbon dioxide emissions arising from the calcination process [2]. In addition to the lower processing temperature and lower limestone content required in the production of wollastonite, wollastonite is able to sequester carbon dioxide by about 18% [2]. The combined effect of the above-mentioned factors is that the embodied carbon of the wollastonite binders is about 70% less than that of OPC, thus, making it desirable as a low carbon binder material [2]. Because of its good fluxing properties, low volatile contents, and needle-like shape which provides a reinforcing capability, wollastonite is also used in the production of ceramics and plastics [5,6]. Carbon dioxide activated

* Corresponding author.
E-mail address: a.ghahremani@miami.edu (A. Ghahremaninezhad).

https://doi.org/10.1016/j.conbuildmat.2023.134243
Received 6 August 2023; Received in revised form 12 September 2023; Accepted 16 November 2023
Available online 24 November 2023

Table 1
Oxide composition of wollastonite powder.

Oxide	SiO_2	CaO	Al_2O_3	MgO	Fe_2O_3	LOI
%	51.3	44.9	0.9	1.6	< 0.2	1.1

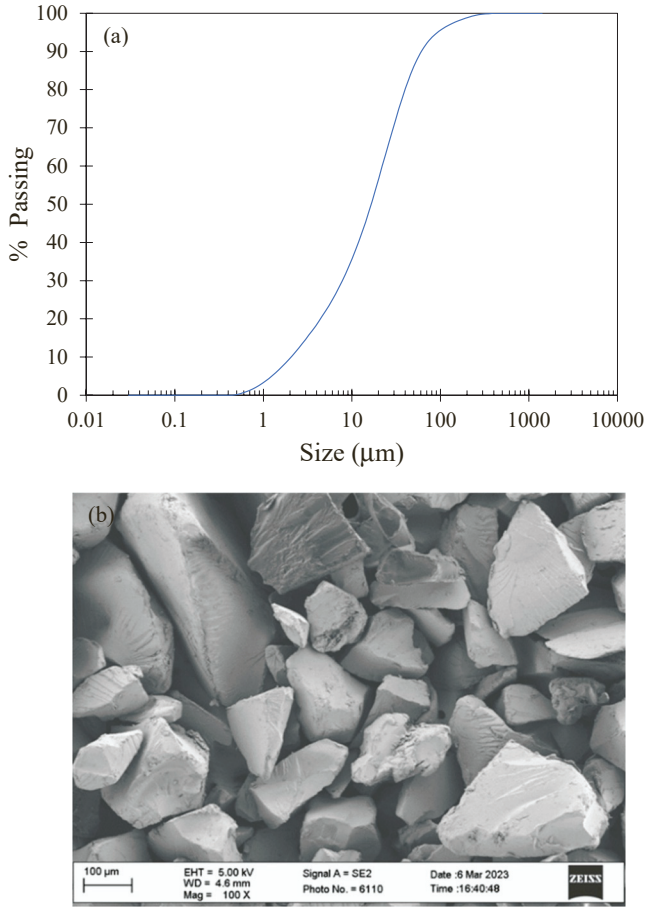

Fig. 1. (a) Cumulative particle size distribution of wollastonite powder. (b) SEM image of hydrogel particles used in the experiments.

wollastonite binders have shown great potentials including higher mechanical properties and superior performance in aggressive environments compared to OPC [7,8]. A compressive strength of 35 MPa was reached after carbonation curing a mortar prepared with wollastonite [9]. Ashraf et al. [2] performed the compressive strength of mortars carbonation cured for 140 h and reported a compressive strength of about 37 MPa.

Carbonation curing at elevated temperatures increases the reaction rate, and as such, has been used in the previous studies [2,10]. However, carbonation at elevated temperatures can also accelerate water evaporation, which can result in drying shrinkage in the carbonated binder. Baffoe and Ghahremaninezhad [8] in a recent investigation observed the formation of drying shrinkage induced cracks in the microstructure of wollastonite binder carbonated at elevated temperature of 55°C. Although many studies concerning the chemical, microstructural and mechanical properties of carbonated wollastonite binders have been conducted [2,9,11], the shrinkage behavior and strategies for its mitigation have not yet been investigated and are poorly understood.

Superabsorbent polymers (SAP) have been used as an internal curing agent over the years to mitigate drying and autogenous shrinkages in alkali activated slag and OPC binders [12–15]. SAP used in construction materials belongs to hydrogels with a large water retention capacity [16–18]. When added to the mixture, hydrogels absorb water and gradually release the water back into the surrounding matrix as the reaction continues and the matrix loses moisture thereby maintaining relative humidity or delaying moisture loss [19–21]. To the best of our knowledge, there have been no studies on the effect of hydrogels on reducing drying shrinkage of carbonated wollastonite binder. Thus, the novelty of this paper is to address this knowledge gap and investigate the drying shrinkage, compressive strength, chemical phase, and microstructure of wollastonite pastes modified with hydrogels carbonated at an elevated temperature. Fourier transform infrared spectroscopy (FTIR), thermogravimetric analysis (TGA), and X-ray diffraction (XRD) were utilized for chemical analysis. X-ray microcomputed tomography (Micro-CT) and scanning electron microscopy (SEM) were employed to examine the internal microstructure and nitrogen adsorption was used to study the pore structure of the carbonated wollastonite paste.

Table 2
Mix design of the pastes used for the experiment.

Sample designation	Water/ wollastonite	% hydrogel by mass of wollastonite	Deionized water (mL)	Wollastonite (g)
Control (0.4)	0.4	0	240	600
Control (0.55)	0.55	0	240	600
H-0.1% (0.55)	0.55	0.1	330	600
H-0.3% (0.55)	0.55	0.3	330	600

2. Experiment

2.1. Materials

Wollastonite powder (calcium metasilicate) was obtained from Seaforth Mineral and Ore Co., INC USA. The oxide composition of the wollastonite powder evaluated using X-ray Fluorescence Spectrometry (XRF) is presented in Table 1. The mean particle size of the wollastonite powder is 16 μm. The cumulative size distribution of wollastonite powder is shown Fig. 1a.

2.2. Hydrogel

The hydrogels used in the study were prepared in-house. The chemicals used in the hydrogel synthesis were purchased from Sigma-Aldrich. The main monomers used in the hydrogel synthesis were the acrylic acid (AA) and acrylamide (AM) monomers, and the synthesis was performed using the free radical polymerization, as discussed in prior papers [19–21]. First, 80 g of AA was pipetted into 800 mL of deionized water and then, 10.8 g of sodium hydroxide (NaOH) was added to the solution to achieve a partial neutralization of AA. The solution was stirred for five minutes. Then, 80 g of AM and 0.4 g of a crosslinking agent called *N,N′*-methylenebisacrylamide (MBA) were added to the solution and stirred continuously for 30 min to ensure complete dissolution of the chemicals. Then, argon gas was used to purge the solution for 5 min to remove the dissolved gases. After degassing, 1.024 g of ammonium persulfate (APS), as the polymerization initiator, was added to the solution and stirred for an additional 5 min. The solution was poured into glass cylinder molds and placed in an oven at 55 ° C for 6 h for gelation to take place. Then, the hydrogels were removed from the molds and broken into smaller pieces. The pieces were then submerged in water for 24 h to remove all unreacted monomers. Then, the hydrogels were washed with acetone and deionized water and oven-dried at 60 ° C for one week until fully dried. The dried pieces of hydrogels were ground into fine particles using a coffee grinder and sieved using a shaker (RX-29, WS TYLER). The hydrogel particles within the range of 75 μm and 450 μm were used in the experiments. Fig. 1b shows the SEM of the hydrogel particles used in the experiments.

2.3. Sample preparation and carbonation of wollastonite paste

The control wollastonite paste was prepared by rotary-mixing wollastonite powder with deionized water at a water to wollastonite ratios (water/wollastonite) of 0.4 and 0.55 for 3 min. For the hydrogel modified paste, 0.1% and 0.3% hydrogel by mass of wollastonite powder were dry mixed with the wollastonite powder for 5 min. The water/wollastonite for the hydrogel modified pastes was 0.55. The mix designs of the pastes with and without hydrogels are shown in Table 2. After dry mixing, deionized water was added to the wollastonite-hydrogel mix and rotary-mixed for 5 min. The pastes were then poured into prismatic molds of dimensions 25 mm × 75 mm × 25 mm and placed on a vibration table for 2 min to achieve a uniform compaction. The compacted pastes were placed inside a water-jacketed carbonation chamber set at a relative humidity (RH) of 95%, a temperature of 50 ºC and carbon dioxide concentration of 20%. The pastes were then demolded after 29 h of carbonation curing and placed back inside the carbonation chamber for the carbonation process to continue except pastes used in the micro-CT analysis to be discussed later in Section 3.6. On the 20th day of carbonation curing, the prismatic pastes were cut into 25 mm × 25 mm × 25 mm cubes using a dry diamond saw. The paste cubes were used for the compressive strength tests. Small pieces obtained from the central portion of the broken cubes were ground into fine powder, passed through the sieve # 60, dried in a vacuum oven at a temperature of 55ºC, and used in FTIR, TGA, XRD, and nitrogen adsorption. For the water loss experiments, 50 g of each of the mixes was spread on a petri dish and tamped gently to ensure that the paste fills the petri dish. Care was taken to ensure that the thickness of the wollastonite paste was approximately 4 mm. The small paste thickness was used in water loss measurement to ensure uniform carbonation in the paste thickness. Right after this process, the pastes were clearly labelled and placed inside a water-jacketed carbonation chamber. The condition of the carbonation process was the same as that used in the prismatic pastes described above.

2.4. Methods

2.4.1. Hydrogel absorption using the teabag test

Hydrogel absorption in the extracted pore solution and deionized water was measured using the teabag test. The teabag test has been widely used in studying the absorption of hydrogels in construction materials [1,22]. To extract pore solution, a mixture with a water/-wollastonite of 0.55 was prepared. Approximately 30 min after the wollastonite and water came into contact, the mixture was filled into 50 mL centrifuge tubes and centrifuged at 5000 RPM for 5 min after which the supernatant was collected. The reason for preparing the pore solution 30 min after wollastonite and water were mixed is that the absorption and solution uptake of hydrogels typically occurs within the first 30 min. The extracted pore solution was quickly transferred into polypropylene tubes to prevent exposure to air. Approximately 0.1 g of hydrogel was placed into teabags and immersed into the extracted pore solution or deionized water. The teabags were removed from the solutions at specific time intervals and their surfaces were dried. The mass of the surface dried teabags was measured using an analytical balance with a resolution of 0.001 g. To account for the quantity of extracted pore solution or deionized water absorbed by the teabag, the mass of the wet teabags without hydrogel was determined by submerging five dry teabags without hydrogel in extracted pore solution or deionized water and the average mass was measured. The hydrogel absorption was monitored until 80 min when the results were seen to stabilize. The hydrogel absorption was determined as follows (3):

$$Q = \frac{M_w - M_{wt} - M_s}{M_s} \quad (3)$$

where M_w, M_{wt}, M_s are the mass of the wet teabags containing hydrogel, wet teabags without hydrogel, and dry hydrogel, respectively. Absorption test was conducted using 5 replicates.

2.4.2. Flow test

The flow test was performed with all mix designs to estimate the flowability of the paste with or without hydrogel. A cone with a bottom diameter of 100 mm, a top diameter of 70 mm and a height of 50 mm was filled with the paste and allowed to rest on a table for 3 min. After 3 min, the cone was removed, and the table was dropped 25 times with a consistent rate over a 15 s period. The average perpendicular diameter of the spread was measured. The flow test was conducted using 3 replicates for each mix design.

2.4.3. FTIR

FTIR was employed to investigate the chemical phases of the carbonated pastes. Approximately, 1 g of the fine powder was utilized in the test. FTIR measurements were performed using a Perkin Elmer Paragon 1000 FTIR with an ATR accessory in the transmission mode. The scan resolution was 4 cm^{-1} and spectra were recorded between 600 cm^{-1} and 4000 cm^{-1}. Each sample was taken through 4 scans and an average of two samples from the 4 rounds of scans was reported for analysis.

2.4.4. TGA

TGA was used to investigate the mineralogical composition of the carbonated pastes. Approximately 30 mg of the sample was loaded into the TGA pan. Samples were scanned using the Netzsch TG at a heating rate of 20 ºC/min and in the temperature range of 24 ºC to 900 ºC. Two replicates of each sample were used, and the average reported.

2.4.5. XRD

The XRD analysis of the carbonated pastes was studied using the Rikagu X-ray Diffractometer (Model D/Max-3 C, Rikagu, Japan). The spectra were obtained using the Cu Kα radiation (40 kV, 20 mA), a scan interval of $2\Theta = 10^{o}$ to 40^{o}, and a step size of 0.02^{o}. Approximately 2 g of the powder was loaded into a sample holder, inserted into the device, and scanned.

2.4.6. SEM

The SEM images of the fracture surfaces of the compressive strength test samples were obtained using a Zeiss Gemini Ultra Plus FESEM in the secondary electron mode. The samples for the SEM were gold coated to decrease the effect of charging. Images were taken at a magnification of 20 kX and an accelerating voltage of 10.00 kV.

2.4.7. Micro-CT analysis

A Bruker SkyScan 1273 (Bruker, Kontich, Belgium) was used to nondestructively evaluate the internal microstructure of the carbonated pastes with and without hydrogel. Scanning was conducted at a resolution of 30 μm / pixel with a 2 mm Copper filter. The micro-CT analysis of the pastes was done after 29, 96, 216 and 480 h of carbonation. The pastes used in the micro-CT imaging had dimensions of 25 mm × 75 mm × 25 mm. The rotational step, exposure time, voltage and current were 0.5^{o}, 1650 ms, 120 kV and 115 μA, respectively. The samples were held firmly in a polypropylene tube filled with a styrofoam and positioned between an X-ray source and an X-ray detector. The samples were scanned for a period of approximately 3 h during which about 200 projections over 180^{o} were taken. The reconstruction was performed using the Bruker software CTAnalyzer 1.20.8. The segmentation of the images into a solid matrix and voids/cracks was done using the greyscale intensity thresholds with the grey scale range of 0–70 representing voids/cracks.

2.4.8. Drying shrinkage

The shrinkage of the carbonated wollastonite paste due to loss of moisture was investigated. Wollastonite paste carbonated for 29, 96, 216 and 480 h were scanned using micro-CT. After scanning and

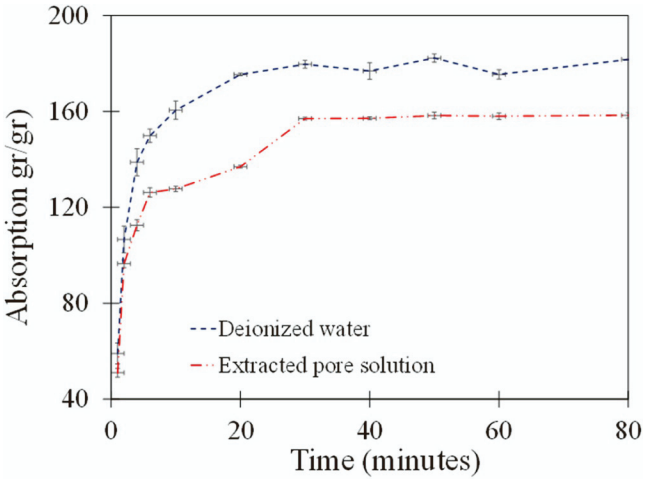

Fig. 2. Absorption behavior of hydrogel in different solutions.

subsequent reconstruction of the paste, 20 reconstructed 2-D slices along the longitudinal axis of each paste were selected, and their area measured using the Image J software to obtain the average cross-sectional area of each sample. The change in the cross-sectional area of the 25 mm by 25 mm paste at different carbonation times was used to determine the areal shrinkage (% mm^2/mm^2) of the pastes. An average of 20 cross-sections of each paste were used and the average reported.

2.4.9. Mass loss

In order to shed light onto the rate of moisture evaporation from the paste during the carbonation process, the change in the mass of the thin pastes was monitored. The sample preparation for the thin pastes was described earlier in Section 2.2. It must be pointed out that the change in mass of the paste is attributed to a mass loss due to moisture evaporation as well as mass increase due to carbonation and calcium carbonate formation. Assuming a similar mass increase due to carbonation, the change in mass can be used to provide an approximate indication of the relative rate of moisture evaporation of the pastes. The use of thin pastes was motivated to provide a uniform carbonation in the pastes. The mass loss of the carbonated paste was determined after 0.5, 2, 3, 4, 6, 24, 72, 96 and 168 h of carbonation time. Three replicates of each sample were used in this experiment and the average reported.

2.4.10. Nitrogen adsorption

Nitrogen adsorption-desorption measurements were carried out using the Anton Paar Physisorption Analyzer instrument. The tests were performed on fine ground carbonated powders prepared as described previously. The samples were weighed and placed inside a tube which was then loaded into the degassing port of the instrument. The sample was degassed at 105 °C until the required vacuum was reached. The degassing process lasted 3 h. Samples were then cooled with liquid nitrogen and analyzed by measuring the volume of nitrogen gas adsorbed at specific pressures. The specific surface area of the samples was calculated using the BET method [23]. The pore size distribution of the samples available to the nitrogen was determined using the Barret, Joyner, Hallenda (BJH) method [24].

2.4.11. Compressive strength

The compressive strength of the carbonated wollastonite cube pastes with and without hydrogel was measured after 20 days of carbonation curing. The compressive strength test was performed using a SATEC testing machine at a loading rate of 0.05 mm/sec. Five replicates of each sample were tested, and the average reported.

Table 3
Flow of wollastonite pastes.

Paste	Immediately (cm)	After 1 h (cm)	After 3 h (cm)
Control (0.4)	20.6	20.2	20.2
Control (0.55)	32.1	32	32.3
H-0.1% (0.55)	26.8	27.4	27.8
H-0.3% (0.55)	16.2	19.4	19

3. Results and discussions

3.1. Teabag and flow test

The absorption capacities of the hydrogel in deionized water and extracted wollastonite pore solution evaluated by the teabag method are shown in Fig. 2. As shown, hydrogel absorption in both solutions reached a plateau at about 30 min after hydrogel contact with the respective solutions and did not change for the rest of the experiment. It can be observed that the absorption capacity of hydrogel in extracted wollastonite pore solution is slightly lower than that in deionized water and this can be attributed to the difference in osmotic pressure between the extracted pore solution and deionized water [22,25,26]. Further, the cation present, in this case, Ca^{2+} may electrostatically interact with the negatively charged carboxylate group of AA and form crosslinks which can inhibit the movement of the polymer network and reduce the absorption capacity of the hydrogel [12]. The effect of pH and ionic strength on the absorption of hydrogels has been extensively studied in the past [22,25,26]. It should be mentioned that unlike hydrogel absorption in extracted pore solution of OPC, hydrogel absorption in the extracted wollastonite pore solution was high. This indicates the markedly lower ionic concentration in the wollastonite pore solution compared to the cement pore solution [8].

Table 3 shows the flow values of the wollastonite paste with and without hydrogel. The flow test was performed at 0 min, 1 h, and 3 h of mixing. It is seen that Control (0.4) showed the lowest flow due to the lower content of water and it stayed the same after 3 h of resting. This confirms that the wollastonite paste is non-hydraulic binder and the water added to the paste remained as free water without carbon curing. Control (0.55) showed a higher flowability, and this was due to the higher amount of water in this mixture. The hydrogel modified paste showed a reduced flowability during time 0 due to the absorption of water from the paste by the hydrogel. Since hydrogels could absorb a portion of the mixing water, the effective water/wollastonite of the wollastonite paste decreased and that was the main reason for why the hydrogel modified paste showed decreased flowability [27]. After 1 and 3 h of resting, it is seen that the flow of the hydrogel modified paste

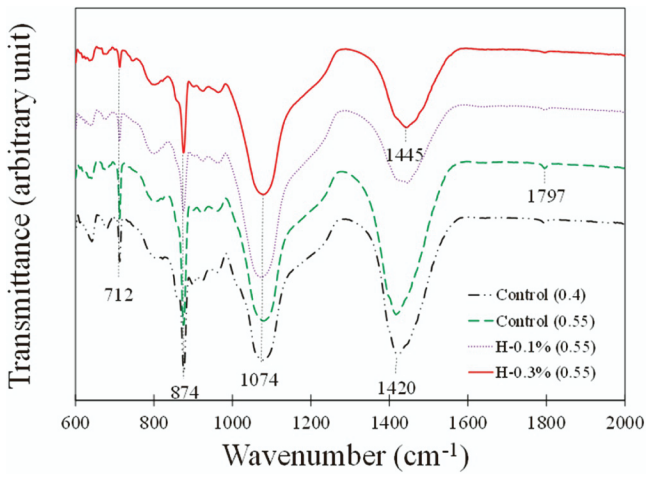

Fig. 3. FTIR results of the carbonated pastes with and without hydrogel.

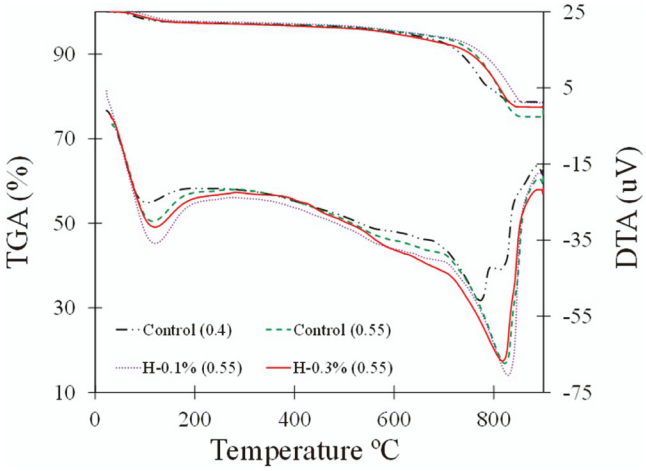

Fig. 4. TGA/DTA curves of the carbonated pastes with and without hydrogel.

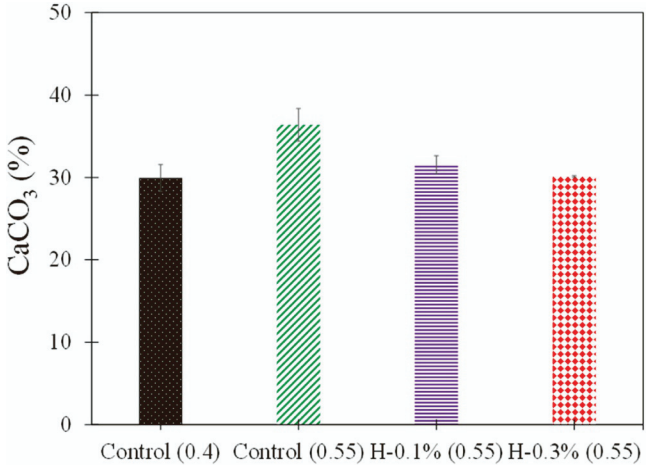

Fig. 5. $CaCO_3$ content of the carbonated pastes.

increased, especially in H-03% (0.55). This is attributed to the release of the solution from the hydrogel into the surrounding wollastonite paste with time. The release behavior of hydrogel in the wollastonite paste can be explained due to a slight increase in the ionic content in the pore solution. as more ions are dissolved from wollastonite into the solution. With an increase in the ionic content of the pore solution with time compared to time 0, a new chemical potential gradient is developed driving the release of solution from the hydrogel into the surrounding pore solution.

3.2. FTIR

FTIR was performed to identify the phase characteristics of $CaCO_3$ formed in the carbonated wollastonite paste with and without hydrogel. Shown in Fig. 3 are the spectra of the carbonated paste after 480 h of carbonation curing. The peaks below 700 cm^{-1} are the characteristic peaks of raw wollastonite and other uncarbonated phases such as quartz, anorthite which are added impurities during production [28]. There are noticeable broad peaks between 800 cm^{-1} and 1200 cm^{-1} corresponding to the asymmetrical stretching vibration of the Si—O bond in the wollastonite. The sharp peaks located at 712 cm^{-1} and 874 cm^{-1} correspond to the presence of calcite [29,30]. The calcite peak was seen to be sharper in the control paste than in H-0.1% (0.55) and H-0.1% (0.4). Control (0.55), however showed the sharpest peaks corresponding to calcite. This could be an indication that calcite was more dominant in the control paste than in the paste modified with hydrogels. The carbonation of calcium silicates comprises two different stages; the initially fast carbonation reaction stage of the calcium silicates is dominated by the chemical kinetics followed by the slower reaction which is influenced by the product-layer diffusion [31,32]. The high moisture content available at the initial stages of the carbonation reaction might have influenced the stabilization or promoted calcite formation in the control. The hydrogel absorbed a part of the solution as indicated by the differences in the flowability results shown in Table 3. As the paste dries out, hydrogel releases some amount of water into the surrounding microstructure. However, the lower amount of water in the hydrogel modified pastes compared to the control paste at early age could result in a slightly lower amount of calcite in the hydrogel modified pastes compared to the control paste [2]. In addition, the relatively slow desorption of water from the hydrogel during the early stages of carbonation reaction may inhibit the provision of water necessary to complete the transformation of ACC and other metastable phases into calcite. The broad band at 1074 cm^{-1} is assigned to the asymmetric stretching vibration of ($\nu 3$) of the Si—O bond [10]. As shown in the FTIR results, a peak occurred at 1420 cm^{-1} for the control pastes and 1445 cm^{-1} for the hydrogel modified pastes. The relatively narrow peak located at 1420 cm^{-1} for the control paste indicates the dominance of calcite in the microstructure of the control paste [29]. While for the hydrogel modified paste the broad peak located at 1445 cm^{-1} indicates some amount of ACC in the microstructure of these pastes. The peak at 1797 cm^{-1} is assigned to the presence of $CaCO_3$ [29] and it was shown to be more intense in the control paste than in the hydrogel modified paste.

3.3. TGA/DTA

TGA and differential thermal analysis (DTA) were employed to investigate the mineralogical phases of the carbonated wollastonite paste with and without hydrogel. DTA measures endo- and exothermic event temperatures and indicates phase transitions while the TGA measures the change of mass with respective to temperature change. Fig. 4 illustrates the TGA/DTA curves after 480 h of carbonation period. The weight loss of the paste at the temperature of 120 °C can be attributed to the evaporation of free water from the paste and the loss of weakly bound water on the gel solid, which is physically adsorbed [33,34]. A minor weight loss is seen to have occurred in the hydrogel modified paste within the range of about 540 ºC to 620 ºC. The weight loss within this region can be attributed to the decomposition of metastable phases or poorly crystalline phases including ACC, vaterite or aragonite in the hydrogel modified paste [11,35,36]. These phases, however, appear to be small as they did not show up in the FTIR spectra. As the temperature was increased, it is noticed that there was a sharp weight loss within the temperature range of 750 ºC and 850 ºC which is considered to be the decarbonation of calcite [37]. The Control (0.4) paste is seen to show this peak at 760 ºC while the Control (0.55) and H-01% (0.55) showed these peaks at an average temperature of about 820 ºC. The endothermic DTA curve at 120 ºC and between 650 ºC and 850 ºC indicates that the thermal decomposition was initiated at a slow rate and experienced rapid decomposition with increasing temperature beyond 700 °C. The variation in peak intensity provides insight into the extent of carbonation of the wollastonite in these pastes. To this end, the amount of total $CaCO_3$ was calculated and quantified using the weight loss between 650 ºC and 850 ºC. Fig. 5 illustrates the total amount of $CaCO_3$ in each paste. It is seen that the Control (0.4) paste showed the lowest amount of $CaCO_3$, and this can be attributed to the faster drying and absence of water, which consequently resulted in reduced carbonation reaction in this paste. Carbonation is influenced by moisture content in the paste as the uptake of CO_2 is influenced by the availability and amount of free water present. The rate of evaporation and drying out is expected to be faster in the Control (0.4) than the rest of the paste. The early carbonation reaction of wollastonite paste is affected by the dissolution of Ca^{2+} and silicate ions, therefore the decreased ionic

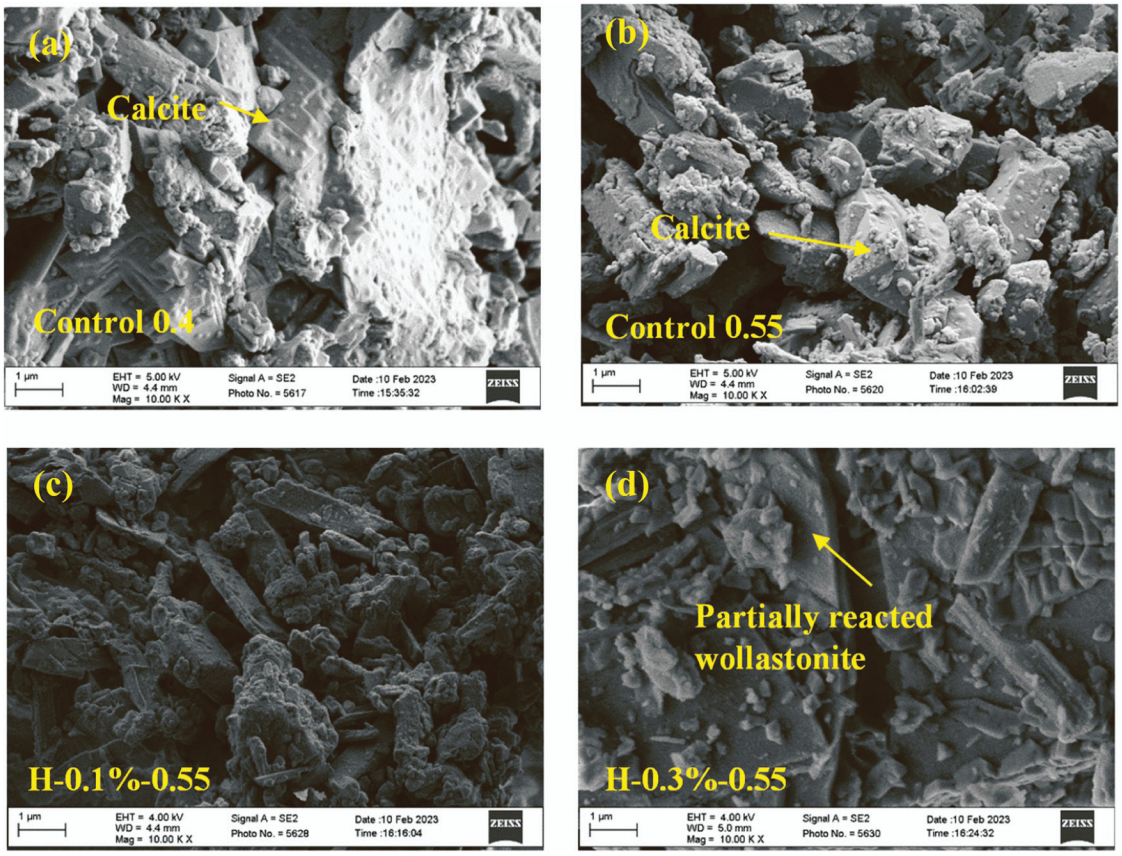

Fig. 6. SEM images showing the microstructure of the carbonated pastes with and without hydrogel.

exchange due to drying out of the paste is likely to delay or reduce the carbonation of $CaSiO_3$ and retard the formation of $CaCO_3$. The H-03% (0.55) is also seen to show a lower total amount of $CaCO_3$. The reason is attributed to the low effective water/wollastonite presents during the early ages of carbonation reaction. Although a water/wollastonite of 0.55 was used in this paste, the 0.3% hydrogel is seen to absorb a large amount of the water as revealed in Table 3 and only released the water in small quantities during the drying out of the specimen. As noted, carbonation reaction is intense at the early stages of reaction; hence, the limited quantity of water during this period may slightly reduce carbonation [2] which is consistent with the FTIR results. It is seen that the Control (0.55) showed the highest total $CaCO_3$ content, and this can be attributed to the presence of a higher water content during the carbonation reaction.

3.4. SEM

The SEM of the fractured surfaces of the 480-hour carbonated paste is shown in Fig. 6. The microstructure of a carbonated paste shows different phases such as partially reacted/unreacted wollastonite particles, calcium modified silica gel, amorphous calcium carbonate (ACC) and crystalline $CaCO_3$ [38]. Generally, the pastes with and without hydrogel showed the dominant formation of calcite, an indication that the sample underwent a high degree of carbonation reaction. This is in support of the observations made by [2,34] that calcite is the primary polymorph of carbonated wollastonite paste. There are also a large number of spherical and granular features seen in the microstructure of all pastes, which are attributed to calcium modified silica gel and potentially a small amount of amorphous calcium carbonate. In the case of the control paste with water/wollastonite of 0.55, the calcites appeared to exhibit slightly larger sizes compared to the control with water/wollastonite of 0.4 and these calcites assumed a rhombohedral

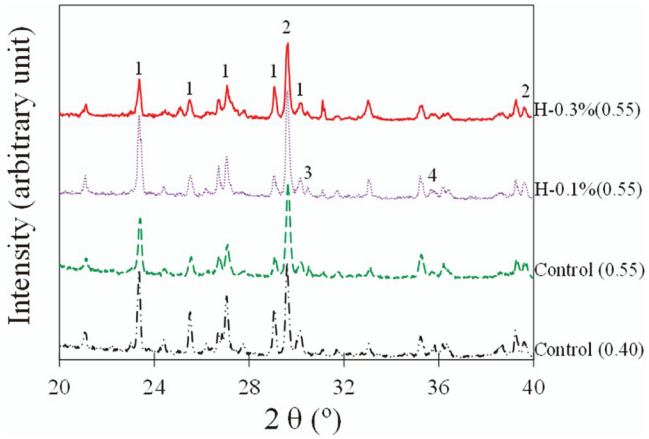

Fig. 7. XRD spectra of the carbonated pastes with and without hydrogel. The peaks numbered 1, 2, 3 and 4 correspond to wollastonite, calcite, aragonite and vaterite, respectively.

shape. The dominance of calcite in the Control (0.55) is consistent with the FTIR and TGA results and may be due to the higher moisture content in the paste during the initial stages of the carbonation reaction [2]. It has been reported that the presence of moisture affects the morphology of the $CaCO_3$ [34]. In this case, it is seen that moisture content was shown to influence the sizes of the calcites.

3.5. XRD

The XRD spectra of the carbonated pastes with and without hydrogel are shown in Fig. 7. The XRD pattern supported the findings in FTIR as it

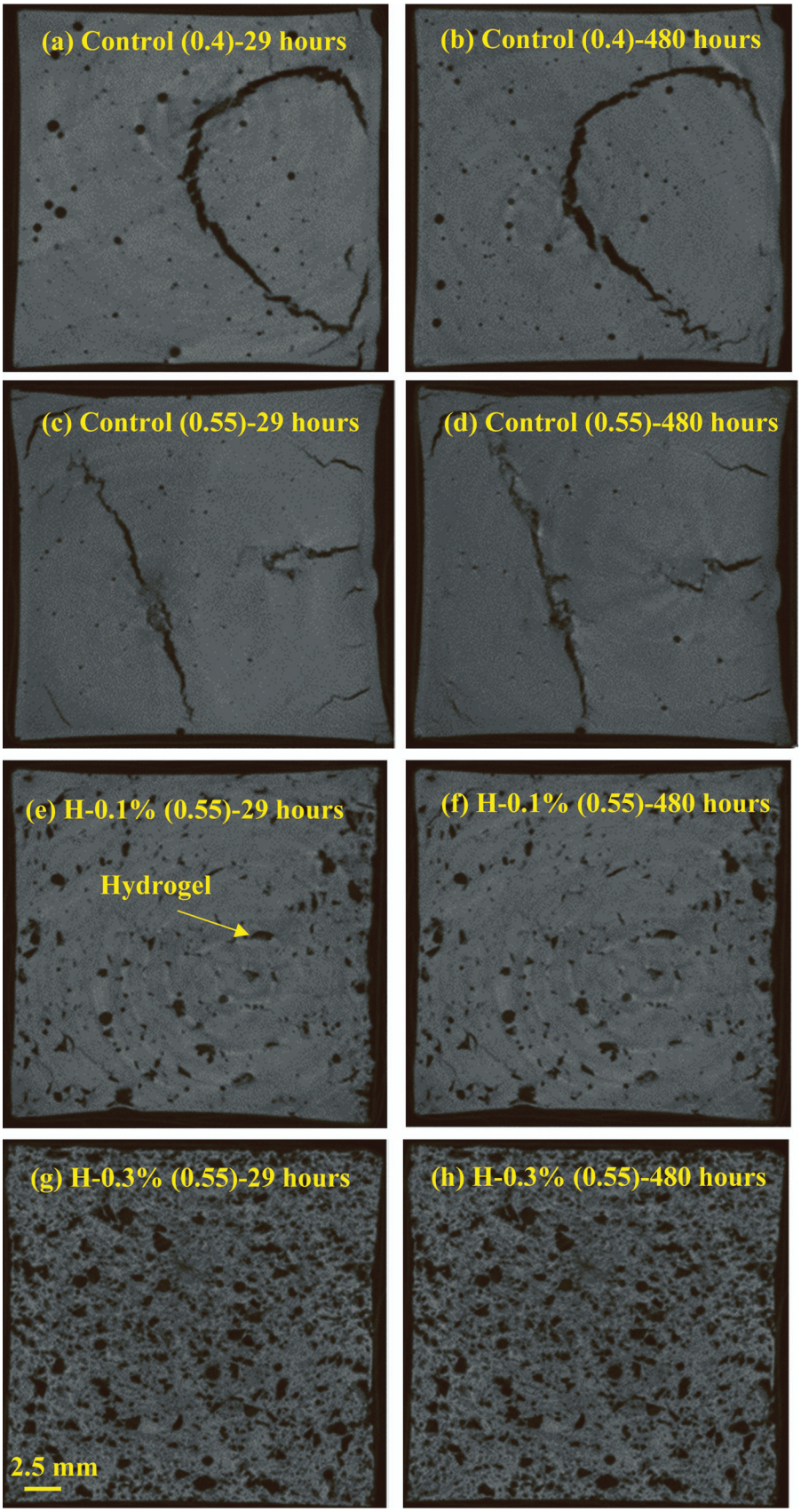

Fig. 8. Micro-CT slices showing cracks and macrovoids in the microstructure of the carbonated pastes. The scale bar is the same for all images.

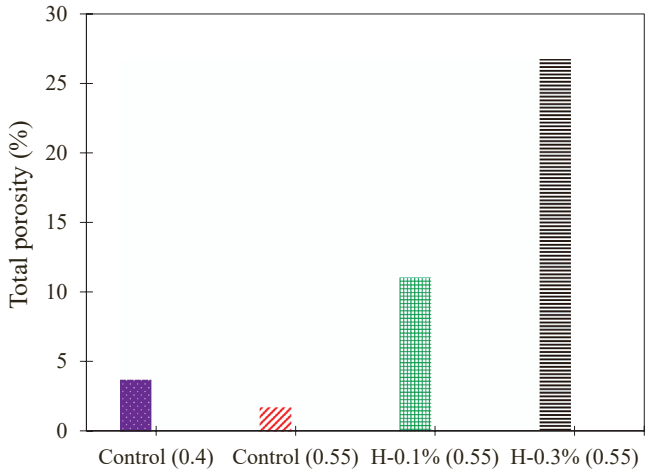

Fig. 9. Total porosity of the voids larger than 30 μm in the pastes.

revealed the main mineralogical phases corresponding to both the control pastes and the hydrogel modified pastes. The XRD spectra showed the presence of crystalline $CaCO_3$ and wollastonite phases. Silica gel was not identified in the XRD spectra because of the amorphous nature of the phase. The peaks numbered 1, 2, 3 and 4 correspond to wollastonite, calcite, aragonite and vaterite, respectively. The wollastonite showed peaks at 2 θ of 23.2°, 2 θ of 25.3°, and 2 θ of 26.9°. The crystals of $CaCO_3$ were identified in three different polymorphs which are 2 θ of 29.4, 2 θ of 35 and 2 θ of 30.5° representing calcite, aragonite and vaterite, respectively. The peaks corresponding to vaterite, and aragonite appeared weak, an indication that the main crystal phase of $CaCO_3$ present was calcite as revealed in the FTIR and SEM results shown in Figs. 3 and 6, respectively. The presence of ACC was difficult to identify due to the small content and the lack of crystallinity.

3.6. Micro-CT analysis

Micro-CT examination was carried out to investigate the internal microstructural characteristics of the carbonated pastes with and without hydrogel. The 2-D reconstruction slices of 29 and 480-hour carbonated pastes are shown in Fig. 8. There are spherical air voids distributed in the microstructure of the pastes and the presence of these air voids is more dominant in Control (0.4). The macrovoids generated in the microstructure as a result of hydrogel desorption are evident in the images corresponding to the hydrogel modified pastes. There are more such macrovoids seen in H-0.1% (0.55) than H-0.3% (0.55). The control pastes at both water/wollastonite and times of carbonation showed the formation of cracks. It is noted that there was not a change in crack formation between the 29-hour and the 480-hour carbonated samples. This indicates that the cracks formed during the early ages, and they could have possibly been formed before the 29-hour duration. The crack formation is attributed to drying shrinkage because of the evaporation of moisture from the paste due to the increased temperature and CO_2 exposure. The water loss results in the formation of capillary tension in the pore solution of the pastes. The capillary tension in the pore solution pulls on the solid skeleton in the microstructure of the paste resulting in the dimensional changes in the paste [8]. When constrained, drying shrinkage leads to the development of tensile stresses in the paste. When the developed tensile stress exceeds the strength of the carbonated paste, cracks start to form. Noticeably, the carbonated paste modified with hydrogel did not show cracks or showed a few much smaller cracks. The significant reduction in cracks in the carbonated paste modified with hydrogel can be attributed to the reduced drying shrinkage as a result of the release of water from the hydrogel into the surrounding microstructure. During the initial carbonation stage where carbonation reaction is more intense, the release of water into the surrounding wollastonite paste partly compensates for water loss, thus, reducing the development of the capillary stresses and crack formation [39]. The total porosity of the voids with a size larger than 30 μm, (including air voids and hydrogel macrovoids) in the control paste and paste modified with hydrogel is shown in Fig. 9. The analysis was done using the 480-hour carbonated pastes. The hydrogel modified pastes showed a higher total porosity than that of the control paste due to increased formation of hydrogel macrovoids in the former. The hydrogel absorption and desorption during the carbonation reaction is responsible for the macrovoid formation [12]. The lower water/wollastonite and flow of the mixture Control (0.4) could facilitate the entrapment of air pockets during mixing in this paste.

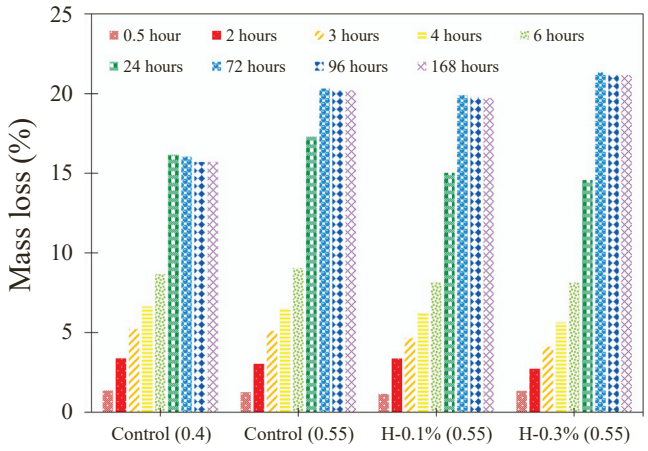

Fig. 10. Mass loss of carbonated pastes with time.

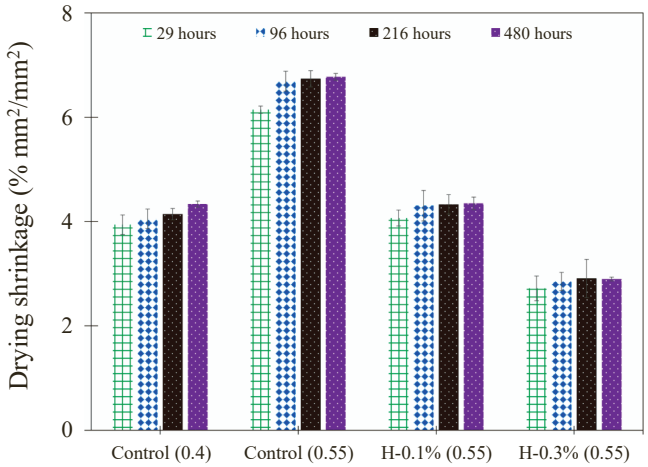

Fig. 11. Drying shrinkage of the carbonated pastes with time.

3.7. Drying shrinkage and mass loss

During the carbonation curing process, the high temperature and CO_2 exposure of the carbonation chamber subject the paste to drying shrinkage due to the evaporation of water from the capillary pores. Due to the structural differences between the silica gel phases, the chemically bound water in wollastonite paste is not as high as in OPC and slag pastes, consequently, the free water remains as interstitial water [40]. In view of this, the moisture loss is expected to be higher in the carbonated wollastonite paste due to the low amount of chemically bound water. The mass loss and drying shrinkage of the carbonated paste are shown in Figs. 10 and 11, respectively. The mass loss due to water evaporation is seen to increase with time. At 0.5 h, carbonated pastes showed a small

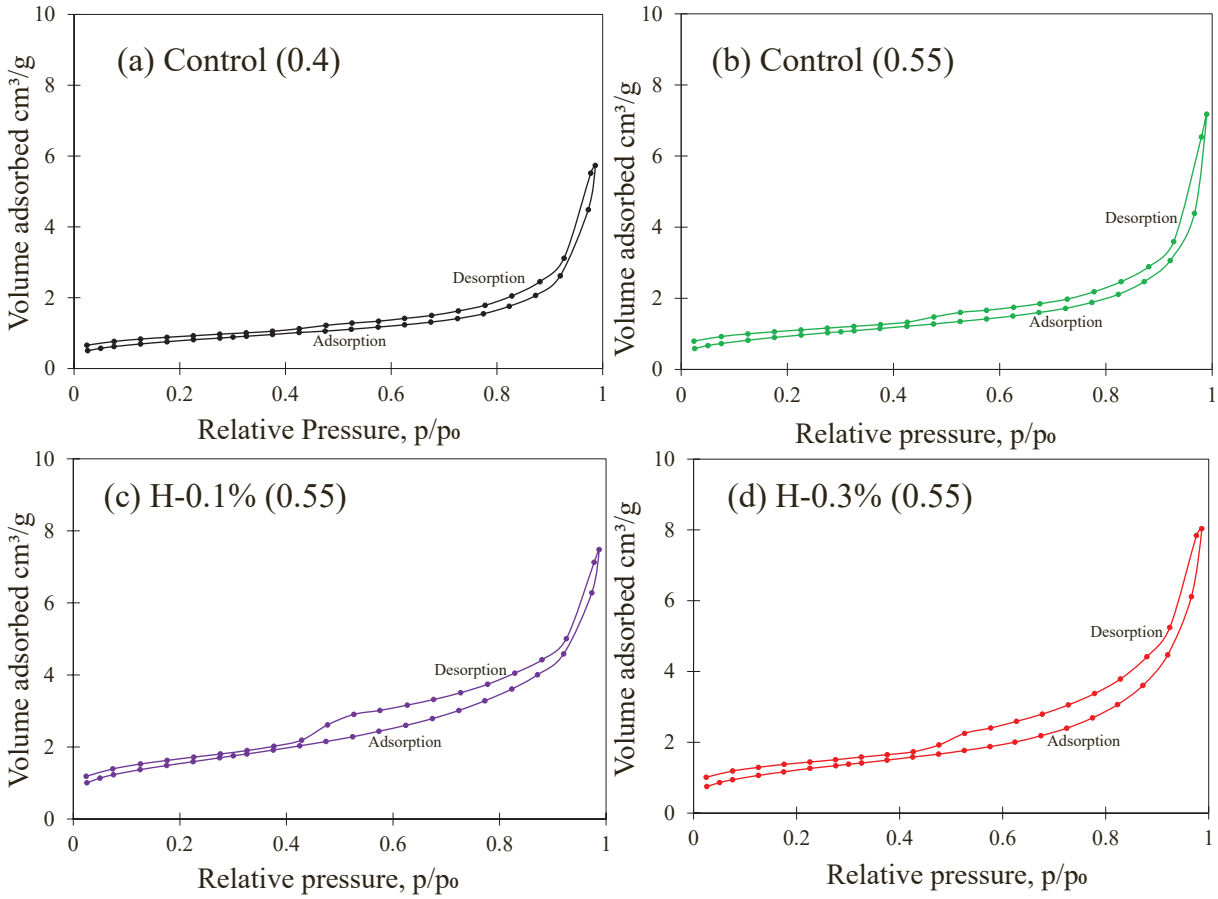

Fig. 12. Adsorption-desorption isotherms of the carbonated pastes.

mass loss, approximately less than 2% but as the carbonation time increased, mass loss increased as well. The mass loss of Control (0.4) was seen to stabilize after 24 h due to the complete drying out of the paste. Control (0.55) continued to show mass loss of water until 72 h of of carbonation time after which it remained unchanged. This is possibly a result of the continuous evaporation of moisture from the paste due to the high water content. The mass loss of water of Control (0.55) and hydrogel modified paste, however, stabilized after 72 h of carbonation. At this time the carbonation reaction is slowed [41]. It is observed that the mass loss in the hydrogel modified pastes was lower than in Control (0.55) and Control (0.4) at 24 h. This indicates that hydrogel was able to reduce water loss at the early age of carbonation. The mass loss change between 24 h and 72 h is more in the hydrogel modified pastes compared to in the Control (0.55). This can be attributed to the continuous release of water from the hydrogel into the carbonation paste as carbonation proceeded after 24 h.

Fig. 11 shows the drying shrinkage of the carbonated pastes at different times of carbonation. Control (0.55) showed the highest shrinkage and H-0.3% (0.55) showed the lowest shrinkage among the pastes. Comparing the shrinkage results to the water loss results discussed previously, it is observed that while the mass loss was the highest in Control (0.55) and lowest in H-0.3% (0.55), drying shrinkage was the highest in the Control (0.55) and lowest in H-0.3% (0.55) at after 29 h of carbonation. This provides an indication that the loss of moisture was a contributing factor to drying shrinkage. It is noted that drying shrinkage did not change significantly in most pastes after 29 h of carbonation. The addition of hydrogel demonstrated its effectiveness in reducing drying shrinkage of the pastes. The reduction in drying shrinkage when hydrogel was mixed with the wollastonite is due to the gradual release of water from the hydrogel into the carbonated paste which maintains the internal relative humidity of the paste and reduces drying shrinkage [42]. The capillary stress development in the pastes due to low internal humidity is responsible for drying shrinkage [14,43]. The mass loss and drying shrinkage results at early age (less than 29 h) follow a similar trajectory and that the quantity of water evaporated from the paste correlated with the shrinkage in the paste. This indicated that the majority of drying shrinkage occurred at the early age. After 96 h, the drying shrinkage seemed to remain unchanged similar to what occurred in the mass loss measurement in Fig. 10.

3.8. Nitrogen adsorption-desorption

The nitrogen adsorption analysis has been used extensively to reveal the porous structural characteristics of materials [44]. In the present work, the nitrogen adsorption isotherms were measured to investigate the porous structural characteristics of Ca-modified silica gel in carbonated calcium silicate. The adsorption-desorption isotherms of carbonated calcium silicate are shown in Fig. 12. The isotherms followed the characteristic pattern of meso-macro porous matrix [45]. Hysteresis loops between desorption-adsorption isotherms were noticed to form for all the carbonated paste. The specific surface area and pore volume of the carbonated paste with and without hydrogel are shown in Figs. 13a and 13b, respectively. Control (0.55) exhibited a slightly higher specific surface area and pore volume than Control (0.4); this is due to the higher initial water content in this paste that allows for a higher carbonation reaction and increased formation of Ca-modified silica gel that are the main contributor to the specific surface area and volume of the pores in the size range of less of 80 nm. It is seen that the hydrogel modified pastes, H-0.1% (0.55) and H-0.3% (0.55) exhibited a higher specific surface area and pore volume compared to Control (0.4) and Control

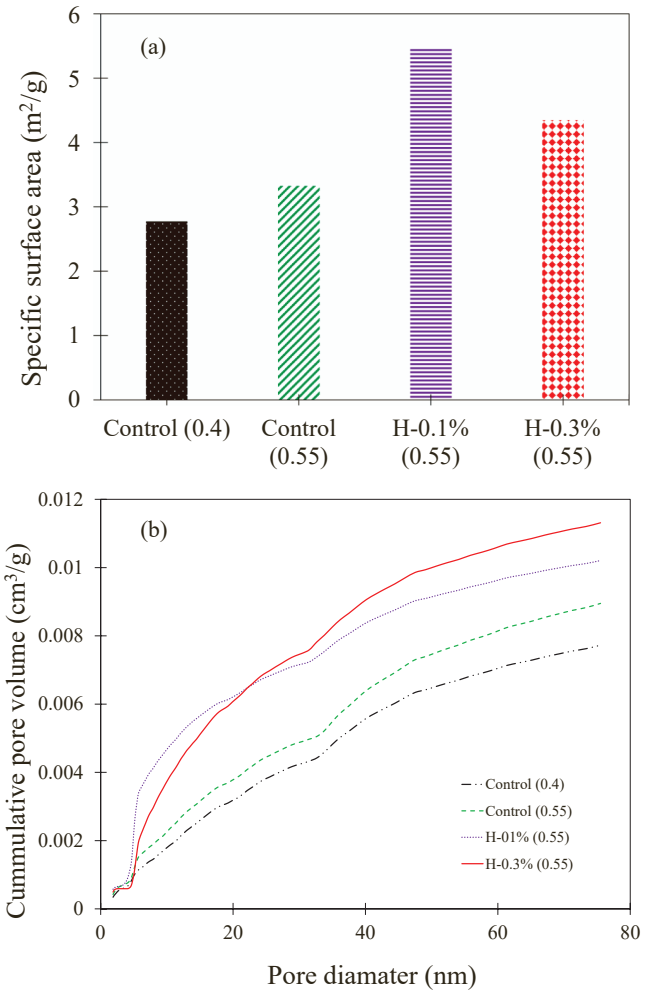

Fig. 13. (a) BET specific surface area and (b) pore volume of the carbonated pastes with and without hydrogels.

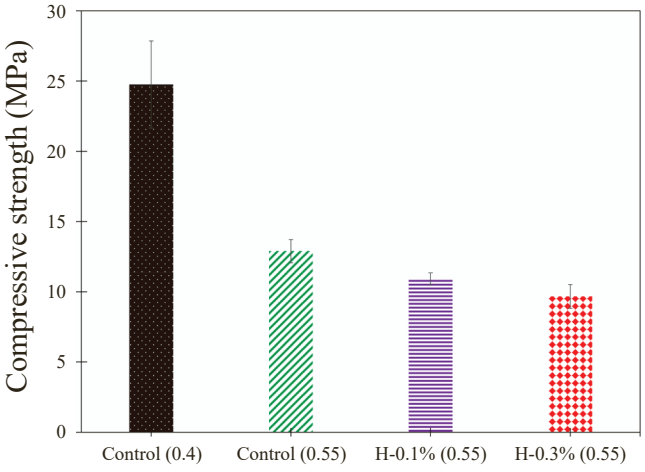

Fig. 14. Compressive strength of the carbonated pastes.

(0.55).

The pores in a carbonated paste can be summarized into the following categories based on pore diameter; the inter-cluster spaces with diameter less than 2 nm, gel pores with diameter between 2 and 10 nm, capillary pores between 10 and 41 nm and large pores greater than 41 nm [34,46]. The intercluster spaces are suggested to contain chemi-sorbed and physi-sorbed water within and in the outer layer of Ca-modified silica gel clusters [34]. In particular, the volume fraction of the pores in the range of 4–20 nm seemed to be noticeably higher in the hydrogel modified pastes compared to the pastes without hydrogels. The reason for this could be attributed to the delayed loss of water due to gradual release of water from the hydrogels into the surrounding matrix.

3.9. Compressive strength

The effect of hydrogel on the compressive strength of carbonated wollastonite paste is shown in Fig. 14. It is seen that the compressive strength of the control pastes is higher than that of the hydrogel modified pastes. This is primarily due to the presence of macrovoids formed in the microstructure of the hydrogel modified pastes as a result of the absorption and desorption of hydrogel. These macrovoids serve as stress concentration sites, which reduce the strength of the paste [47]. The reduction in compressive strength due to the formation of macrovoids in cementitious materials has also been documented in the previous studies [1,47,48]. It is to be noted that despite a high porosity of macrovoids caused by hydrogels, the pastes with hydrogels, H-0.1% (0.55) and H-0.3% (0.55) showed a relatively small reduction in compressive strength compared to Control (0.55). This can be attributed to the presence of cracks in Control (0.55), as shown in Fig. 8, markedly reducing compressive strength in this paste. The compressive strength of Control (0.4) is higher than that of Control (0.55) due to a lower water/wollastonite and lower total capillary porosity in this paste. Ashraf et al. [2] investigated the compressive strength of carbonated wollastonite mortar at different water/wollastonite and reported a higher compressive strength for the mortar with lower water/-wollastonite. They attributed the increase in compressive strength with decreasing water/wollastonite to decreasing total capillary porosity. It should be noted that both Control (0.4) and Control (0.55) experienced cracking as demonstrated in Fig. 8, which is expected to negatively influence compressive strength in these pastes.

4. Conclusions

The influence of hydrogel on the microstructure and properties of carbonated wollastonite pastes was examined. The following conclusions are drawn from the study:

- Hydrogel absorption was lower in the extracted pore solution of the wollastonite paste than in deionized water; however, hydrogels showed significantly higher absorption in the pore solution of wollastonite paste than in the pore solution of OPC paste, which provides indirect evidence for a lower ionic strength, particularly lower Ca^{2+} concentration in the pore solution of the wollastonite paste compared to OPC paste. The flow test results also indicated high absorption of hydrogel in wollastonite paste.
- FTIR, TGA, and XRD showed the presence of calcite, as the primary polymorph in the carbonated wollastonite paste. Control (0.55) exhibited higher calcite content compared to hydrogel modified pastes most likely due to the availability of higher content of free water which enhanced the carbonation reaction at the initial stages of the carbonation reaction. SEM imaging provided evidence for larger calcite particles in Control (0.55) compared to the hydrogel modified pastes.
- The micro-CT examination of the carbonated pastes revealed the presence of cracks in the control pastes while no or significantly fewer cracks were observed in the hydrogel modified pastes. Cracking was caused by drying shrinkage in the control carbonated pastes and hydrogel was effective in mitigating such cracking by lowering water loss at early stage of carbonation.
- The nitrogen adsorption analysis showed a higher specific surface area and pore volume corresponding to the pores smaller than 80 nm in the hydrogel modified pastes compared to the control.

- The hydrogel modified pastes exhibited a slightly lower compressive strength compared to the control paste due to the presence of macrovoids.

CRediT authorship contribution statement

Ghahremaninezhad Ali: Writing – review & editing, Writing – original draft, Project administration, Methodology, Investigation, Funding acquisition, Formal analysis, Data curation, Conceptualization. **Baffoe Elvis:** Writing – original draft, Formal analysis, Data curation.

Declaration of Competing Interest

The authors declare that they have no known competing financial interests or personal relationships that could have appeared to influence the work reported in this paper.

Data Availability

Data will be made available on request.

Acknowledgements

This study was supported in part by the National Science Foundation under the CAREER award number 1846984. The X-ray micro-CT imaging was made possible by the National Science Foundation under the MRI award number 1920127. Any opinions, findings, and conclusions or recommendations expressed in this material are those of the author(s) and do not necessarily reflect the views of the National Science Foundation.

References

[1] B. Vafaei, K. Farzanian, A. Ghahremaninezhad, The influence of superabsorbent polymer on the properties of alkali-activated slag pastes, Constr. Build. Mater. 236 (2020), 117525, https://doi.org/10.1016/j.conbuildmat.2019.117525.
[2] W. Ashraf, J. Olek, S. Sahu, Phase evolution and strength development during carbonation of low-lime calcium silicate cement (CSC), Constr. Build. Mater. 210 (2019) 473–482, https://doi.org/10.1016/j.conbuildmat.2019.03.038.
[3] W. Ashraf, J. Olek, Carbonation activated binders from pure calcium silicates: Reaction kinetics and performance controlling factors, Cem. Concr. Compos 93 (2018) 85–98, https://doi.org/10.1016/j.cemconcomp.2018.07.004.
[4] W. Ashraf, J. Olek, N. Tian, Multiscale characterization of carbonated wollastonite paste and application of homogenization schemes to predict its effective elastic modulus, Cem. Concr. Compos 72 (2016) 284–298, https://doi.org/10.1016/j.cemconcomp.2016.05.023.
[5] B. Singh, M. Gupta, A. Verma, Polyester moulding compounds of natural fibres and wollastonite, Compos Part A Appl. Sci. Manuf. 34 (2003) 1035–1043, https://doi.org/10.1016/S1359-835X(03)00239-2.
[6] J. Tong, Y. Ma, R.D. Arnell, L. Ren, Free abrasive wear behavior of UHMWPE composites filled with wollastonite fibers, Compos, Part A Appl. Sci. 37 (2006) 38–45, https://doi.org/10.1016/j.compositesa.2005.05.023.
[7] W. Ashraf J. Olek H. Jeong V. Atakan Effects of high temperature on carbonated calcium silicate cement (csc) and ordinary portland cement (OPC) paste Int. Conf. Durab. Concr. Struct., ICDCS 2016 2016 1 7 doi: 10.5703/1288284316153.
[8] E. Baffoe, A. Ghahremaninezhad, Effect of proteins on the mineralization, microstructure and mechanical properties of carbonation cured calcium silicate, Cem. Concr. Compos (2023), 105121, https://doi.org/10.1016/J.CEMCONCOMP.2023.105121.
[9] J.M. Bukowski, R.L. Berger, Reactivity and strength development of CO_2 activated non-hydraulic calcium silicates, Cem. Concr. Res 9 (1979) 57–68, https://doi.org/10.1016/0008-8846(79)90095-4.
[10] W. Ashraf, J. Olek, Carbonation behavior of hydraulic and non-hydraulic calcium silicates: potential of utilizing low-lime calcium silicates in cement-based materials, J. Mater. Sci. 51 (2016) 6173–6191, https://doi.org/10.1007/s10853-016-9909-4.
[11] R.I. Khan, W. Ashraf, J. Olek, Amino acids as performance-controlling additives in carbonation-activated cementitious materials, Cem. Concr. Res 147 (2021), 106501, https://doi.org/10.1016/j.cemconres.2021.106501.
[12] K. Farzanian, B. Vafaei, A. Ghahremaninezhad, The influence of the chemical composition of hydrogels on their behavior in cementitious materials, Mater., Struct. Constr. 54 (2021) 1–19, https://doi.org/10.1617/s11527-021-01838-z.
[13] A. Mignon, D. Snoeck, P. Dubruel, S. Van Vlierberghe, N. De Belie, Crack mitigation in concrete: superabsorbent polymers as key to success? Materials 10 (2017) https://doi.org/10.3390/ma10030237.
[14] A.A. Melo Neto, M.A. Cincotto, W. Repette, Drying and autogenous shrinkage of pastes and mortars with activated slag cement, Cem. Concr. Res 38 (2008) 565–574, https://doi.org/10.1016/j.cemconres.2007.11.002.
[15] S. Oh, Y.C. Choi, Superabsorbent polymers as internal curing agents in alkali activated slag mortars, Constr., Build. Mater. 159 (2018) 1–8, https://doi.org/10.1016/j.conbuildmat.2017.10.121.
[16] Khashayar Farzanian, Ali Ghahremaninezhad, On the effect of chemical composition on the desorption of superabsorbent hydrogels in contact with a porous cementitious material, Gels 4 (2018) 70, https://doi.org/10.1617/s11527-017-1068-9.
[17] K. Farzanian, A. Ghahremaninezhad, Desorption of superabsorbent hydrogels with varied chemical compositions in cementitious materials, Mater. Struct. 51 (2018), 3, https://doi.org/10.1617/s11527-017-1128-1.
[18] Khashayar Farzanian, Ali Ghahremaninezhad, The effect of the capillary forces on the desorption of hydrogels in contact with porous cementitious material, Mater. Struct. 50 (2017), 216, https://doi.org/10.1617/s11527-017-1068-9.
[19] K. Farzanian, A. Ghahremaninezhad, Desorption of superabsorbent hydrogels with varied chemical compositions in cementitious materials, Mater. Struct. /Mater. Et. Constr. 51 (2018) 1–15, https://doi.org/10.1617/s11527-017-1128-1.
[20] K. Farzanian, A. Ghahremaninezhad, The effect of the capillary forces on the desorption of hydrogels in contact with a porous cementitious material, Mater. Struct. /Mater. Et. Constr. 50 (2017) 1–15, https://doi.org/10.1617/s11527-017-1068-9.
[21] K. Farzanian, A. Ghahremaninezhad, On the interaction between superabsorbent hydrogels and blended mixtures with supplementary cementitious materials, Adv. Civ. Eng. Mater. 7 (2018) 1–24, https://doi.org/10.1520/ACEM20180073.
[22] J. Prabahar, B. Vafaei, A. Ghahremaninezhad, The effect of hydrogels with different chemical compositions on the behavior of alkali-activated slag pastes, Gels 8 (2022), https://doi.org/10.3390/gels8110731.
[23] S. Brunauer, P.H. Emmett, E. Teller, Adsorption of gases in multimolecular layers, J. Am. Chem. Soc. 60 (1938) 309–319.
[24] L.G.J, P.P.H. Elliott, P. Barrette, The determination of pore volume and area distributions in porous substances.I. Computations from nitrogen isotherms, J. Am. Chem. Soc. (1951) 373–380, https://doi.org/10.1021/ja01145a126.
[25] K. Farzanian, K. Pimenta Teixeira, I. Perdigão Rocha, L. De Sa Carneiro, A. Ghahremaninezhad, K.P. Teixeira, I.P. Rocha, L.D.S. Carneiro, A. Ghahremaninezhad, K. Pimenta Teixeira, I. Perdigão Rocha, L. De Sa Carneiro, A. Ghahremaninezhad, The mechanical strength, degree of hydration, and electrical resistivity of cement pastes modified with superabsorbent polymers, Constr. Build. Mater. 109 (2016) 156–165, https://doi.org/10.1016/j.conbuildmat.2015.12.082.
[26] B. Vafaei, K. Farzanian, A. Ghahremaninezhad, Effect of hydrogels containing nanosilica on the properties of cement pastes, J. Compos. Sci. 5 (2021) 1–19, https://doi.org/10.3390/jcs5040105.
[27] G. Zhang, H. Xia, W. Zhang, Y. Niu, L. Song, H. Chen, D. Cao, Mechanical properties, drying shrinkage, microstructure of modified cement mortar based on poly(acrylamide-co-methacrylic acid) microgel, Constr. Build. Mater. 284 (2021), 122824, https://doi.org/10.1016/j.conbuildmat.2021.122824.
[28] W. Ashraf, J. Olek, J. Jain, Microscopic features of non-hydraulic calcium silicate cement paste and mortar, Cem. Concr. Res 100 (2017) 361–372, https://doi.org/10.1016/j.cemconres.2017.07.001.
[29] E. Baffoe, A. Ghahremaninezhad, On the interaction between proteins and cracked cementitious surface, Constr. Build. Mater. 352 (2022) 2, https://doi.org/10.1016/j.conbuildmat.2022.128982.
[30] E. Baffoe, A. Ghahremaninezhad, The effect of biomolecules on enzyme-induced calcium carbonate precipitation in cementitious materials, Constr. Build. Mater. 345 (2022), 128323, https://doi.org/10.1016/j.conbuildmat.2022.128323.
[31] P. Sun, J.R. Grace, C.J. Lim, E.J. Anthony, A discrete-pore-size-distribution-based gas-solid model and its application to the CaO + CO_2 reaction, Chem. Eng. Sci. 63 (2008) 57–70, https://doi.org/10.1016/j.ces.2007.08.054.
[32] D. Mess, A.F. Sarofim, J.P. Longwell, Product layer diffusion during the reaction of calcium oxide with carbon dioxide, Energy Fuels 13 (1999) 999–1005, https://doi.org/10.1021/ef980266f.
[33] H. Huang, G. Ye, D. Damidot, Characterization and quantification of self-healing behaviors of microcracks due to further hydration in cement paste, Cem. Concr. Res 52 (2013) 71–81, https://doi.org/10.1016/j.cemconres.2013.05.003.
[34] W. Ashraf, J. Olek, Elucidating the accelerated carbonation products of calcium silicates using multi-technique approach, J. CO_2 Util. 23 (2018) 61–74, https://doi.org/10.1016/j.jcou.2017.11.003.
[35] C.E. Weir, E.R. Lippincott, Infrared studies of aragonite, calcite, and vaterite type structures in the borates, carbonates, and nitrates, J. Res. Natl. Bur. Stand A Phys. Chem. 65A (1961) 173, https://doi.org/10.6028/jres.065a.021.
[36] S. Zdenek, Carbonization of porous concrete and its main binding components, Cem. Concr. Res 1 (1971) 645–662, https://doi.org/10.1016/0008-8846(71)90019-6.
[37] M. Thiery, G. Villain, P. Dangla, G. Platret, Investigation of the carbonation front shape on cementitious materials: Effects of the chemical kinetics, Cem. Concr. Res 37 (2007) 1047–1058, https://doi.org/10.1016/j.cemconres.2007.04.002.
[38] W. Ashraf, J. Olek, Carbonation activated binders from pure calcium silicates: Reaction kinetics and performance controlling factors, Cem. Concr. Compos 93 (2018) 85–98, https://doi.org/10.1016/j.cemconcomp.2018.07.004.
[39] H. Cui, F. Chen, Y. Liao, Z. Liang, L. Luo, X. Wang, H.H. Guo, J. Zhao, G. Meng, G. Ouyang, W. Ke, H.H. Guo, Hydrophobic hydrogels as internal curing agent for concrete: the double benefit of super high water content and excellent anti-ion permeability, Compos. Commun. 33 (2022), 101236, https://doi.org/10.1016/j.coco.2022.101236.

[40] W. Ashraf, J. Olek, V. Atakan, Carbonation reaction kinetics, CO_2 sequestration capacity, and microstructure of hydraulic and non-hydraulic cementitious binders, Sustain. Constr. Mater. Technol. (2016), https://doi.org/10.18552/2016/scmt4s303.
[41] W. Ashraf, A. Dissertation, Reaction kinetics, microstructural features and mechanical properties of CO2 activated low-lime calcium silicate binders, ProQuest. (2017).
[42] X. Ma, J. Liu, Z. Wu, C. Shi, Effects of SAP on the properties and pore structure of high performance cement-based materials, Constr. Build. Mater. 131 (2017) 476–484, https://doi.org/10.1016/j.conbuildmat.2016.11.090.
[43] Z.Y. Qu, Q. Yu, Y.D. Ji, F. Gauvin, I.K. Voets, Mitigating shrinkage of alkali activated slag with biofilm, Cem. Concr. Res 138 (2020), https://doi.org/10.1016/j.cemconres.2020.106234.
[44] H. Hamdan, A mixture model approach to big data clustering and classification, ACM Int. Conf. Proc. Ser. 31 (2016) 883–892, https://doi.org/10.1145/3010089.3016031.
[45] W.E.D, E.T. Stephen Brunauer, Lola S. Deming, On a theory of the van der Waals adsorption of gases, J. Am. Chem. Soc. 1139 (1940).
[46] H.M. Jennings, A. Kumar, G. Sant, Quantitative discrimination of the nano-pore-structure of cement paste during drying: New insights from water sorption isotherms, Cem. Concr. Res 76 (2015) 27–36, https://doi.org/10.1016/j.cemconres.2015.05.006.
[47] J. Prabahar, B. Vafaei, E. Baffoe, A. Ghahremaninezhad, The effect of biochar on the properties of alkali-activated slag pastes, Constr. Mater. 2 (2021) 1–14, https://doi.org/10.3390/constrmater2010001.
[48] M. Kamali, A. Ghahremaninezhad, An investigation into the influence of superabsorbent polymers on the properties of glass powder modified cement pastes, Constr. Build. Mater. 149 (2017) 236–247, https://doi.org/10.1016/j.conbuildmat.2016.02.085.